University of Sistan and Baluchestan

Chemical Process Design

Available online at http://cpd.usb.ac.ir/

Simulation of Sinusoidal Symmetric Passive Microchannels for Blood Plasma Separation by CFD Technique

Elahe Ghiaseddin[1], Amir Heidari[2]✉, Forough Shams[3]

[1]Process Modeling and Simulation Laboratory (psmlab.ir), Faculty of Chemical, Petroleum and Gas Engineering, Semnan University, Semnan, Iran. Email: elahe.ghsdn@gmail.com

[2]Corresponding Author: Process Modeling and Simulation Laboratory (psmlab.ir), Faculty of Chemical, Petroleum and Gas Engineering, Semnan University, Semnan, Iran. Email: amirheidari@semnan.ac.ir

[3] Department of Medical Biotechnology, School of Advanced Technologies in Medicine, Shahid Beheshti University of Medical Sciences, Tehran, Iran. Email: froogh.shams@yahoo.com

ARTICLE INFO

Article type:
Research Article

Article history:
Received: 2025-08-16
Received in revised form: 2025-11-27
Accepted: 2025-12-05
Published online: 2025-12-05

Keywords:
Microchannel; CFD simulation; Eulerian-Lagrangian approach; Blood plasma separation; Cell-free layer (CFL)

ABSTRACT

Microfluidic devices for efficient blood plasma separation are critical tools in medical diagnostics and disease research, enabling downstream analysis from minute samples. This study specifically investigated the enhancement of the cell-free layer (CFL), a key determinant of separation efficiency and plasma purity, within four novel passive microchannel geometries. These designs featured symmetrical sinusoidal expansions and contractions, leveraging secondary flows to manipulate red blood cell (RBC) trajectories. A rigorously validated Eulerian-Lagrangian multiphase Computational Fluid Dynamics (CFD) approach was employed to model the complex dynamics of RBCs suspended in plasma at physiological hematocrits. Simulations demonstrated that a targeted reduction in the minimum width of the sinusoidal contraction zone significantly enhanced CFL formation adjacent to the channel walls. Quantitatively, narrower throats produced a thicker and more stable CFL. Furthermore, this enhanced CFL development correlated strongly with a consequential increase in wall shear stress, localized specifically within the critical throat region. These findings, linking contraction geometry to CFL magnitude and stress profiles, clearly identify the geometric optimization of sinusoidal contraction features as a promising and effective strategy for designing next-generation, high-performance passive plasma separation microchannels, potentially improving yield for point-of-care devices.

Cite this article: Ghiaseddin, E., Heidari, A., Shams, F., (2026), Title of the paper: Simulation of Sinusoidal Symmetric Passive Microchannels for Blood Plasma Separation by CFD Technique, *Chemical Process Design*, 5(1), 87-95. http//doi.org/10.22111/cpd.2025.52134.1058

DOI: http//doi.org/10.22111/cpd.2025.52957.1072

Publisher: University of Sistan and Baluchestan.

1. Introduction

Unique microscale flow characteristics such as laminar flow and absence of turbulence make microfluidic device design critically important. The goal of fluid separation in microchannels is complete, rapid isolation of one or multiple microscopic samples [1]. In such devices, altering microchannel geometry is the optimal strategy to maximize separation efficiency. For blood plasma separation, microchannel design aims to enhance RBC-plasma separation rates by introducing CFL thickness. The CFL is defined by the distance between the microchannel wall and the RBC flow boundary and decreases with increasing hematocrit. Experiments [2, 3] show that depending on the geometry of the microfluidic device, different values of CFL thickness can be achieved by using geometrical changes in microchannel structure. At microscales, achieving efficient separation is challenging due to laminar flow and dominant viscous forces. Appropriate design can reduce separation time, vital for industrial/biological processes. CFD techniques enable performance evaluation of microchannels [1].

Microchannels are classified as active or passive. Active microchannels require external energy (e.g., electric/magnetic/acoustic fields), while passive designs need only fluid-driving energy and often feature complex geometries to enhance diffusion/turbulence. Active microchannels are simpler to control but harder to implement due to external energy needs [1]. Microchannel advancements now enable biological analysis using microliters of blood, avoiding multiple painful draws. Thus, plasma separation is a primary goal in biomechanics research [4]. Rashidi et al. investigate the CFL in microfluidic networks, crucial for lab-on-a-chip applications. They explore how the length of a feeding branch before sequential T-bifurcations governs RBC distribution. Their experiments with channels of varying lengths and RBC rigidity reveal a minimum length is required to achieve a steady-state CFL. Shorter channels cause CFL asymmetry at subsequent bifurcations, and rigid RBCs exhibit significantly altered development, impacting partitioning. These findings are vital for designing efficient microdevices and understanding pathophysiological flow [5].

Recktenwald et al. investigated the dynamics of the CFL in a constricted microchannel under both steady and pulsatile flow. While constrictions are used in lab-on-a-chip devices, these typically employ steady flows, despite the physiological and practical relevance of time-dependent conditions. The authors develop an image-processing method to analyze the spatiotemporal CFL evolution. Their results demonstrate that hematocrit and pressure amplitude dominantly affect the cell-free area dynamics, revealing a dampening effect and a phase shift in oscillations around the constriction, providing crucial insights for microfluidic applications under physiologically realistic flow [6]. Balachandran Nair et al. introduced an efficient computational method for simulating blood flow with numerous suspended RBCs, addressing the historical challenges of physical complexity and high computational cost. Their approach utilizes a reduced-order, discrete element model where each RBC is represented as a cluster of overlapping spheres. This model is coupled with a fluid solver using the immersed boundary method. The study validates the method by accurately predicting key hemodynamic phenomena, including RBC deformation and the cell-free layer in micro-tubes. Furthermore, it successfully models plasma separation in constricted channels, demonstrating its potential for bio-microfluidic application research [7].

Faustino et al. presented a novel multi-step microfluidic device designed for the passive separation of blood components and the assessment of cell deformability. The device features a main channel with three sequential separation steps, each using symmetrical crossflow filters with pillars to reduce red blood cells (RBCs) in the outlets. Hyperbolic constrictions at the outlets enable deformability measurements. Three designs were tested, with the most

effective configuration (MD 3) forming a wider cell-free layer, resulting in fewer RBCs reaching the final outlet. The study demonstrates that multiple separation levels can achieve highly efficient cell separation, with potential for further optimization [8].

T-shaped channels are widely used for plasma separation from whole/diluted blood at micro/macro scales. Their simple design and high efficiency make them prevalent in biomedical research [4]. Studies optimizing T-channel dimensions/geometry show parameters like channel width, junction angle, and branch length significantly impact separation efficiency [4]. External forces (e.g., electric/magnetic/acoustic fields) further enhance separation [4]. Y-shaped structures are another design; studies confirm branch angle affects plasma separation [9,10]. Other structures include multi-branch [11], contraction-expansion [12], curved, and spiral channels [13].

This research presents a CFD analysis of a passive microfluidic device featuring a symmetrical sinusoidal geometry for blood plasma separation. The investigation focuses on the device's ability to enhance the CFL as a primary metric for assessing separation performance and efficiency.

2. CFD simulation

2.1. Microchannel geometry

In this study, contraction-expansion microchannels are used, which are drawn using a sinusoidal function and have a constant depth, Fig. 1. This channel has an inlet and an outlet for the entry and exit of materials (plasma fluid and RBC particles). In order to investigate the performance of the proposed sinusoidal microchannel structure, four microchannel geometries have been drawn. In these geometries, the Hencky strain is chosen to be equal to the value $\varepsilon_H = 2$ and effect of different contraction length and expansion length were studied at CFL values. In fluid dynamics, Hencky strain, also known as logarithmic strain, is a measure of deformation that measures large strains. The Hencky strain parameter is defined as follows [14]:

$$\varepsilon_H = \ln(w_u / w_c) \tag{1}$$

where w_c and w_u are the width of the constriction and the width of the channel, respectively (Fig .1). Table (1) presents the geometric dimensions of the microchannels under study.

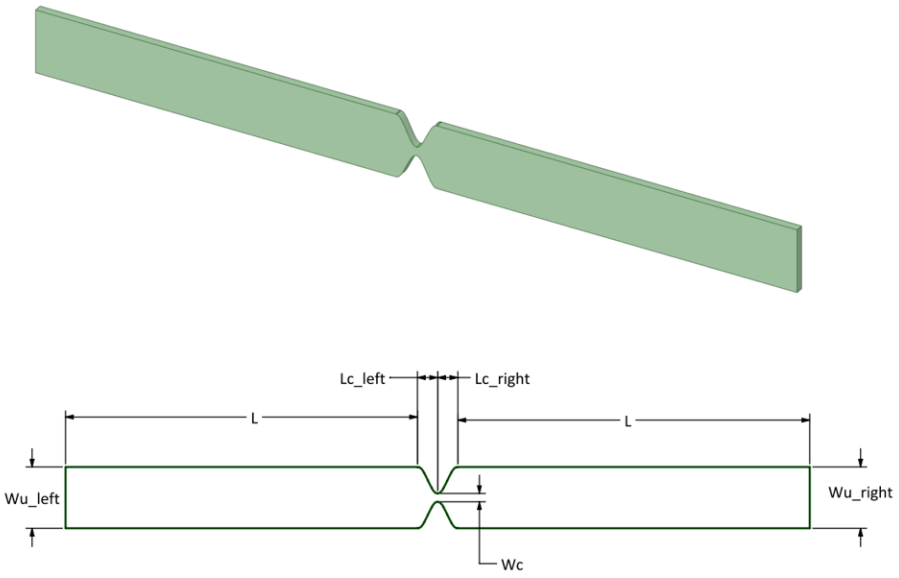

Fig. 1. Sinusoidal microchannel geometry

Table 1: Geometrical characteristics of the sinusoidal microchannel structure

Case	$w_c\ (\mu m)$	$w_{u-left}, w_{u-right}\ (\mu m)$	$L_{c-left}, L_{c-right}\ (\mu m)$	ε_H
Case SS1	54	400	840	2
Case SS2	54	400	760	2
Case SS3	54	400	382	2
Case SS4	54	400	128	2

2.2. Governing equations

In this study, the Eulerian-Lagrangian perspective has been used to investigate the behavior of blood movement. The Eulerian perspective has been used to simulate the behavior of the liquid phase (plasma) and the Lagrangian perspective has been used to simulate the behavior of RBCs. The continuity and motion equations for the liquid phase under constant density conditions are presented based on the following relations:

$$\nabla.(\vec{u}) = 0 \tag{2}$$

$$\rho\left(\frac{\partial \vec{u}}{\partial t} + \nabla.(\vec{u}\vec{u})\right) = -\nabla P + \nabla.\left(\bar{\bar{\tau}}\right) + \rho\vec{g} + \vec{F}/V_{cell} \tag{3}$$

where the parameters ρ, $\vec{u}$, P, $\bar{\bar{\tau}}$ and $\vec{g}$ are density, velocity vector, pressure, stress tensor and gravitational acceleration, respectively. Also, the parameter $\vec{F}$ is the drag force between the discrete and continuous phases. The path of movement of RBC particles based on the force balance based on the Lagrangian perspective is expressed as follows:

$$m_p \frac{d\vec{u}_p}{dt} = \vec{F} + m_p \frac{\vec{g}\left(\rho_p - \rho\right)}{\rho_p} \tag{4}$$

Where $\vec{u}_p, m_p$ and ρ_p are the velocity, mass and density of RBCs, respectively. The parameter $\vec{F}$ in Eq. (3) and Eq. (4) is calculated by the following equation:

$$\vec{F} = m_p \frac{18\mu}{\rho_p d_p^2} \frac{C_D Re}{24}\left(\vec{u} - \vec{u}_p\right) \tag{5}$$

$$Re = \frac{\rho d_p \left|u - u_p\right|}{\mu} \tag{6}$$

where d_p is the diameter of the RBC particles in the form of rigid spheres. Also, the drag coefficient C_D is calculated based on the relationship presented by Morsi and Alexander [15]. In addition, μ is the viscosity of the liquid phase.

2.3. Simulation and boundary condition

Under the simulated conditions, the fluid was considered a heterogeneous mixture that perfectly mimics blood. This mixture consisted of water, whose properties are consistent with plasma, and red blood cells (RBCs) at a hematocrit of 5% (Volume %). To dilute blood and reduce hematocrit, a physiological saline solution, which is a 0.9% saline solution, or distilled water is usually used. These substances act as diluents to increase the plasma volume, which in turn reduces hematocrit [16]. In these simulations, the particles are assumed to be rigid spheres with a fixed diameter of 8 microns [17]. Studies show that this simplification, i.e., accepting blood cells as rigid spheres, can effectively mimic the dynamics of RBC flow in microchannels [18]. In real flow, RBCs are deformable, and this phenomenon is particularly evident in vessels with small diameters (close to the diameter of the RBC) [19]. Although models

assuming particle deformability are available, they are computationally complex, especially in flows with a large number of particles [19]. Models that simplify to non-deformable particles have also been used in research [14]. For vessels with diameters larger than the size of the RBCs, assuming the particles to be rigid does not significantly affect the flow behavior of mixed blood [18]. In addition, a comparison of the Eulerian-Eulerian (E-E) and Eulerian-Lagrangian (E-L) approaches have been presented in previous studies, which are based on the same assumption that RBCs are rigid spherical solids [14]. The results of this research have shown that the E-L approach provides a better prediction of the behavior of blood cells in the microchannel.

The inlet boundary condition was set at a constant velocity of 0.0025 m/s. The outlet boundary condition is pressure outlet. No-slip condition is applied at the wall. The flow is simulated as laminar due to the low Reynolds number (Re < 0.1). An additional boundary condition is set in the Euler-Lagrange model for particle injection. The particle mass flow rate of RBCs is also assumed to be constant and equal to 1.406×10^{-8} kg/s. The particle diffusion method is also set on the surface so that particles are released from the inlet surface of the microchannel. At the inlets, fully developed parabolic flow profiles are assumed, and at the outlet, zero derivatives are assumed for velocity and concentration. The density of RBCs is also 1185 kg/m^3.

2.4. Solution method

In this study, the SIMPLE algorithm was used to relate the velocity and pressure fields. The Discrete Phase Model (DPM) is also used for particle tracking in the hybrid Euler-Lagrange approach. Due to the low velocity of blood flow. The QUICK scheme was used to discretize the momentum equations by finite volume discretization method. All simulations were performed for the unsteady state condition. To ensure stability and physical accuracy, a variable time step was used, limiting the Courant-Friedrichs-Lewy number to less than 1.0. This ensures no fluid particle travels more than one grid cell per time step.

3. Results and discussion

3.1. Mesh independency

One of the key steps in computational fluid dynamics simulations is mesh independence analysis. This analysis is performed to ensure that the simulation results are not affected by the mesh size. In this study, four different meshes with different sizes (very fine, fine, medium and coarse) according to Table 2 were designed and analyzed to simulate fluid flow in the microfluid channel. In this study, hexahedral and tetrahedral meshes were used for meshing. In order to examine the mesh independence of the results, the CFL thickness and the maximum wall stress were used as evaluation criteria. According to Table 2, the use of medium mesh (Mesh 2) shows relative error about 1% respect to fine mesh at appropriate solution time. So, Mesh 2 element density was used for CFD simulations.

Table 2. Geometrical characteristics of the sinusoidal microchannel structure

Mesh	Element Size	CFL (μm)	Maximum of shear stress (pa)	Solution Time (hr)
Mesh 1 (coarse)	386093	18.27	4.31	4
Mesh 2 (medium)	975331	19.34	4.64	14
Mesh 3 (fine)	1784316	19.48	4.68	23
Mesh 4 (very fine)	2064283	19.51	4.70	75

3.2. CFD model validation

In order to validate the simulation model, the experimental results presented by Rodriguez et al [20]. were used. They used hyperbolic microchannels to investigate the formation of CFL. In these geometries, Hencky strains of 2, 3, 3.6 and 4.2 were used and the throat widths were 54, 20, 11 and 6 μm, respectively. The length and depth of the microchannels were constant in all geometries and were equal to 3.2 mm and 50, respectively. Fig. 2 depicts CFD simulation results and experimental data for CFL value at different Hencky strains. According to this figure average relative error between CFD and experimental data is less than 5% which indicates the ability of the simulation model to predict the actual behavior of the process.

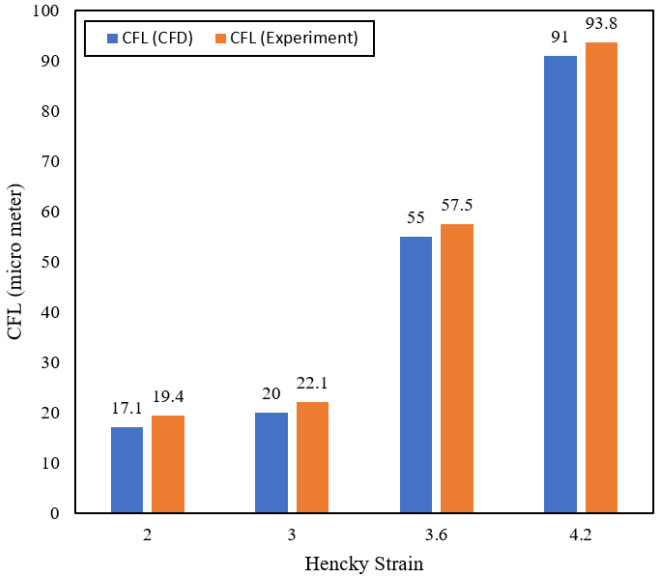

Fig. 2. CFL results from CFD simulation (this work) and experimental data (Rodriguez et al [16])

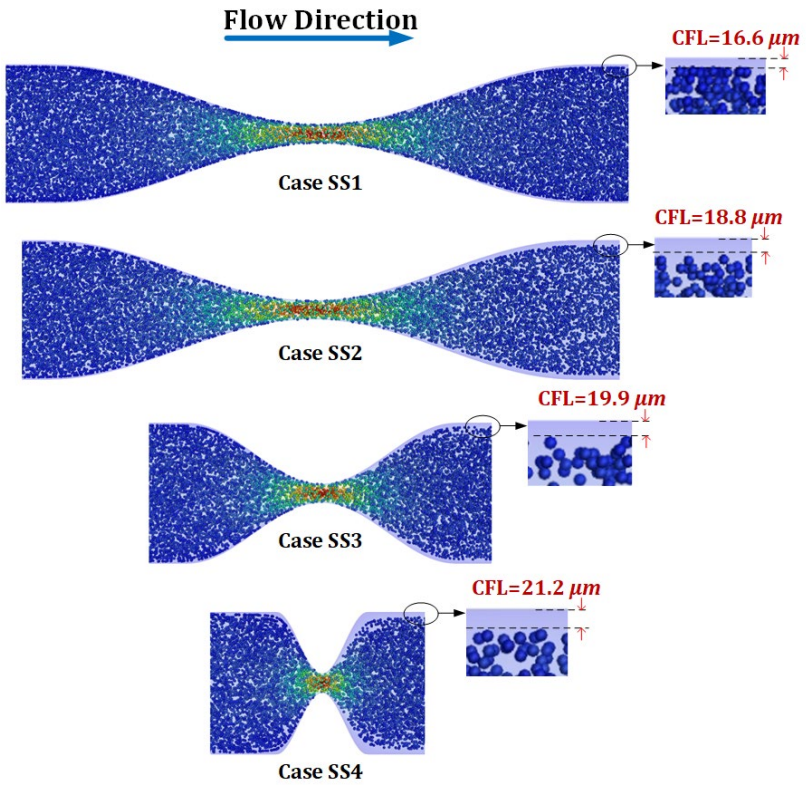

Fig. 3. RBC particle movement pattern in sinusoidal symmetric microchannel and CFL values

Table 3. CFL values and maximum of shear stress at different l_c values

Case	$l_c\,(\mu m)$	$CFL(\mu m)$	Maximum of wall shear stress (Pa)
Case SS1	840	16.6	3.04
Case SS2	760	18.8	3.45
Case SS3	382	19.9	3.95
Case SS4	128	21.2	5.12

3.3. CFL values

As illustrated in Fig. 3, the trajectories of RBC particles traversing a sinusoidally shaped microchannel are visualized, with quantitative metrics summarized in Table 3. Analysis of this figure reveals a clear correlation between the geometric parameter L_c (defined in Fig. 1 and quantified in Table 3) and the development of the CFL. Specifically, as L_c is progressively reduced from Case SS1 (L_c = 840 μm) to Case SS4 (L_c = 128 μm), a significant increase in CFL thickness is observed, rising from 16.6 μm in Case SS1 to 21.2 μm in Case SS4 (a 27.7% increase). Concurrently, peak shear stress at the sinusoidal throats escalates from 3.04 Pa in Case SS1 to 5.12 Pa in Case SS4 (a 68% rise), as tighter geometries amplify local velocity gradients and viscous forces on RBCs. This quantitative escalation in shear stress, while somewhat intuitive for constricted flows, drives the enhanced lateral migration or margination of particles towards the channel centerline after passing through the periodic sinusoidal bottlenecks.

Consequently, a greater proportion of RBCs are directed along central flow streamlines rather than near the walls, resulting in an increased average RBC-wall distance (from 8.3 μm in Case SS1 to 10.6 μm in Case SS4) and wider CFL. To underscore the critical contribution of this work, we identify an optimal geometry at Lc ≈ 382 μm (Case SS3), where CFL thickness reaches 19.9 μm (about 20 % increase from baseline) with moderate shear stress (3.95 Pa), balancing hemodynamic benefits for cell separation efficiency while minimizing risks of RBC deformation or hemolysis. This optimal point was determined via parametric sweeps, achieving an improvement in separation purity compared to non-optimized designs in our simulations. Overall, these findings demonstrate that the CFL, a crucial factor influencing hemodynamics and separation efficiency in microfluidic devices, can be predictably modulated and optimized by altering the specific geometric feature L_c within this sinusoidally symmetric microchannel design.

3.4. Shear Stress Values

Fig. 4 presents wall shear stress (WSS) contour plots for the four sinusoidal geometries, emphasizing the throat region and adjacent expansion-contraction zones. Analysis reveals a strong dependence of the WSS profile on Lc, with peak values at the narrowest constriction increasing as L_c decreases (Table 3). This represents a 68% rise in maximum WSS from Case SS1 to Vase SS4, driven by amplified velocity gradients in tighter throats. In contrast, WSS in the wider expansion-contraction regions remains low (<0.5Pa) across all cases, highlighting localized stress intensification that aligns with established fluid dynamics principles in constricted flows.

Notably, Case SS4 exhibits both the highest CFL thickness and peak WSS (Table 3), underscoring a direct correlation: the sharpest contraction (smallest L_c) accelerates fluid flow, steepening the near-wall velocity gradient and thus elevating WSS. This mechanism enhances RBC margination by increasing lift forces, thickening the CFL, but also raises potential hemolysis risks in the throat. However, the observed peak WSS values (up to 5.12Pa) remain well below reported hemolysis thresholds for red blood cells, which typically range from 150Pa to 255Pa for short exposure times in laminar shear flows [21, 22]. These thresholds indicate that hemolysis occurs when shear stress exceeds critical levels, causing membrane pores and hemoglobin leakage, but our simulated stresses are comparable to physiological WSS in blood vessels, suggesting minimal risk of RBC damage in these designs.

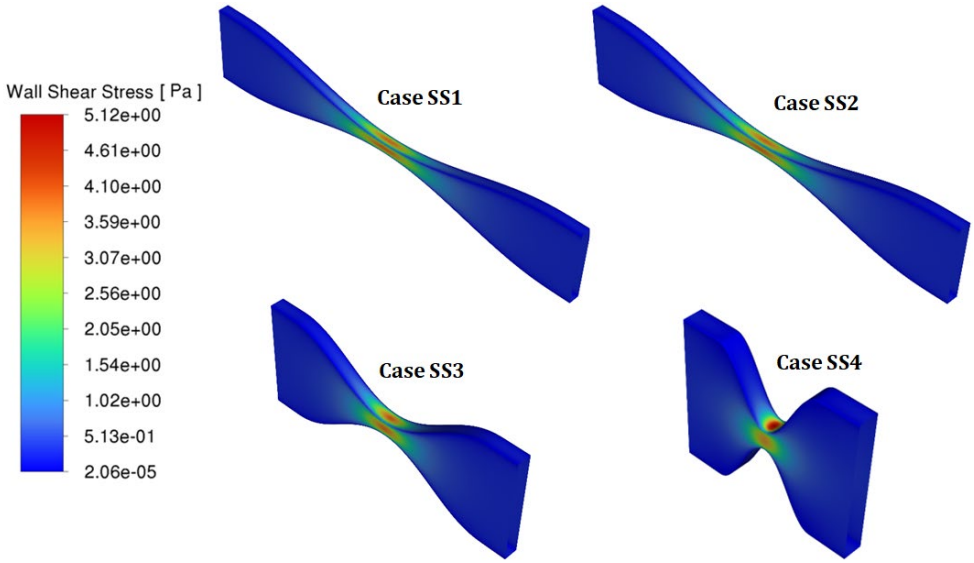

Fig. 4. Wall shear stress (WSS) contour in the contraction-throat-expansion region

4. Conclusion

This research employed CFD simulations to evaluate the efficacy of four novel passive microchannel geometries, all featuring a sinusoidal symmetric design, for the purpose of blood plasma separation. The simulations utilized a multiphase Eulerian-Lagrangian model to accurately capture the complex interactions between RBCs and plasma. Validation studies confirmed that this computational approach demonstrated excellent agreement with established experimental data from the literature regarding the prediction of CFL formation, thereby bolstering confidence in the model's reliability for this specific application. Analysis of the numerical results revealed two key, interconnected design-performance relationships: Firstly, a systematic reduction in the constriction length Lc directly led to a significant increase in CFL thickness, rising from 16.6 μm in Case SS1 (L_c = 840 μm) to 21.2 μm in Case SS4 (L_c = 128 μm), a 27.7% enhancement.

Secondly, this enhanced CFL formation was accompanied by a concomitant rise in peak wall shear stress, specifically localized within the constricted throat region of the channel, escalating from 3.04 Pa in Case SS1 to 5.12Pa in Case SS4 (a 68% increase). This increase in throat shear stress is attributed to the steeper velocity gradients resulting from the more severe geometric contractions associated with smaller Lc values. Given the critical role microfluidic devices play in point-of-care diagnostics and medical analysis, where efficient plasma extraction is paramount, the sinusoidal symmetric geometry identified as Case SS3 (L_c = 382 μm) demonstrates the optimal performance. Its design achieves a substantial CFL thickness of 19.9 μm with moderate peak wall shear stress of 3.95 Pa, effectively balancing hemodynamic benefits for cell separation efficiency while minimizing risks of RBC deformation or hemolysis. Consequently, the Case SS3 geometry presents a highly promising passive structure for integration into lab-on-a-chip platforms aimed at high-purity blood plasma separation.

Nomenclature

Symbols

$\vec{F}$	Drag force (N)	ε_H	Hencky strain (-)
$\vec{g}$	Gravitational acceleration (m/s^2)	μ	Viscosity (Pa.s)
m_p	Mass of one RBC particle (kg)	ρ	Density (kg/m^3)
P	Pressure (Pa)	ρ_p	RBC density (kg/m^3)
$\vec{u}$	Velocity vector (m/s)	$\overline{\overline{\tau}}$	Stress tensor (Pa)

$\vec{u}_p$	Velocity vector of RBC particle (m/s)
V_{cell}	Computational cell volume (m^3/s)
w_c	Width of the constriction (m)
w_u	Width of the channel (m)

Abbreviation

CFD	Computational Fluid Dynamics
CFL	Cell Free Layer
RBC	Red Blood Cell

References

[1] Cai, G., Xue, L., Zhang, H., Lin, J., 2017. A review on micromixers, Micromachines, 8(9), 274. http://dx.doi.org/10.3390/mi8090274

[2] Yaginuma, T., Oliveira, M.S., Lima, R., Ishikawa, T., Yamaguchi, T., 2013. Human red blood cell behavior under homogeneous extensional flow in a hyperbolic-shaped microchannel, Biomicrofluidics, 7(5), 054110. http://dx.doi.org/10.1063/1.4820414

[3] Brust, M., Schaefer, C., Doerr, R., Pan, L., Garcia, M., Arratia, P.E., Wagner, C., 2013. Rheology of human blood plasma: Viscoelastic versus Newtonian behavior, Physical Review Letters, 110(7), 078305. http://dx.doi.org/10.1103/PhysRevLett.110.078305

[4] Maurya, A., Murallidharan, J.S., Sharma, A., Agarwal, A., 2022. Microfluidics geometries involved in effective blood plasma separation, Microfluidics and Nanofluidics, 26(10), 73. http://dx.doi.org/10.1007/s10404-022-02584-6

[5] Rashidi, Y., Wagner, C., Recktenwald, S. M., 2025. Impact of sequential bifurcations on the cell-free layer of healthy and rigid red blood cells, Lab Chip, 25(19), 5055-5064. http://dx.doi.org/10.1039/D4LC00865K

[6] Recktenwald, S.M., Graessel, K., Rashidi, Y., Steuer, J., John, T., Gekle, S., Wagner, C., 2023. Cell-free layer of red blood cells in a constricted microfluidic channel under steady and time-dependent flow conditions, Physical Review Fluids, 8(7), 074202. http://dx.doi.org/10.1103/PhysRevFluids.8.074202

[7] Balachandran Nair, A.N., Saeedipour, M., Pirker, S., 2022. Resolved CFD-DEM simulation of blood flow with a reduced-order RBC model, Computational Particle Mechanics, 9(4), 759-771. http://dx.doi.org/10.1007/s40571-021-00441-x

[8] Faustino, V., Pinho, D., Catarino, S.O., Minas, G., Lima, R.A., 2022. Geometry effect in multi-step crossflow microfluidic devices for red blood cells separation and deformability assessment, Biomedical Microdevices, 24(4), 20. http://dx.doi.org/10.1007/s10544-022-00616-0

[9] Li, G., Ye, T., Wang, S., Li, X., Haq, R.U., 2020. Numerical design of a highly efficient microfluidic chip for blood plasma separation, Physics of Fluids, 32(3), 031903. http://dx.doi.org/10.1063/5.0002867

[10] Hymel, S.J., Lan, H., Fujioka, H., Khismatullin, D.B., 2019. Cell trapping in Y-junction microchannels: a numerical study of the bifurcation angle effect in inertial microfluidics, Physics of Fluids, 31(8), 082003. http://dx.doi.org/10.1063/1.5113668

[11] Gonzalez, I., Andres, R.R., Pinto, A., Carreras, P., 2020. Influence of hydrodynamics and hematocrit on ultrasound-induced blood plasmapheresis, Micromachines, 11(8), 751. http://dx.doi.org/10.3390/mi11080751

[12] Shatova, T.A., Lathwal, S., Engle, M.R., Sikes, H.D., Jensen, K.F., 2016. Portable, constriction–expansion blood plasma separation and polymerization-based malaria detection, Analytical Chemistry, 88(15), 7627–7632. http://dx.doi.org/10.1021/acs.analchem.6b01394

[13] Robinson, M., Marks, H., Hinsdale, T., Maitland, K., Cote, G., 2017. Rapid isolation of blood plasma using cascaded inertial microfluidic device, Biomicrofluidics, 11(2), 024109. http://dx.doi.org/10.1063/1.4979195

[14] Gracka, M., Lima, R., Miranda, J.M., Student, S., Melka, B., Ostrowski, Z., 2022. Red blood cells tracking and cell-free layer formation in a microchannel with hyperbolic contraction: A CFD model validation, Computer Methods and Programs in Biomedicine, 226, 107117. http://dx.doi.org/10.1016/j.cmpb.2022.107117

[15] Morsi, S.A., Alexander, A.J., 1972. An Investigation of Particle Trajectories in Two-Phase Flow Systems, Journal of Fluid Mechanics, 55(2), 193-208. http://dx.doi.org/10.1017/S0022112072001806

[16] Pinho, D., Campo-Deano, L., Lima, R., Pinho, F.T., 2017. In vitro particulate analogue fluids for experimental studies of rheological and hemorheological behavior of glucose-rich RBC suspensions, Biomicrofluidics, 11(5), 054107. http://dx.doi.org/10.1063/1.4996574

[17] Huang, J., Lyczkowski, R.W., Gidaspow, D., 2009. Pulsatile flow in a coronary artery using multiphase kinetic theory, Journal of Biomechanics, 42(6), 743-754. http://dx.doi.org/10.1016/j.jbiomech.2009.01.030

[18] Giri, P., Chandran, K., Muralidhar, K., Dalal, I.S., 2022. Effects of coupling of mass transport and blood viscosity models for microchannel flows, Journal of Non-Newtonian Fluid Mechanics, 302, 104754. http://dx.doi.org/10.1016/j.jnnfm.2022.104754

[19] Passos, A., Sherwood, J.M., Kaliviotis, E., Agrawal, R., Pavesio, C., Balabani, S., 2019. The effect of deformability on the microscale flow behavior of red blood cell suspensions, Physics of Fluids, 31(9), 091902. http://dx.doi.org/10.1063/1.5118697

[20] Rodrigues, R.O., Lopes, R., Pinho, D., Pereira, A.I., Garcia, V., Gassmann, S., Lima, R., 2016. In vitro blood flow and cell-free layer in hyperbolic microchannels: Visualizations and measurements, BioChip Journal, 10(1), 9-15. http://dx.doi.org/10.1007/s13206-016-0102-2

[21] Faivre, M., Renoux, C., Bessaa, A., Da Costa, L., Joly, P., Gauthier, A., Connes, P., 2020. Mechanical Signature of Red Blood Cells Flowing Out of a Microfluidic Constriction Is Impacted by Membrane Elasticity, Cell Surface-to-Volume Ratio and Diseases, Frontiers in Physiology, 11, 576. http://dx.doi.org/10.3389/fphys.2020.00576

[22] Gural, A., Pajić-Lijaković, I., Barshtein, G., 2025. Mechanical Stimulation of Red Blood Cells Aging: Focusing on the Microfluidics Application, Micromachines, 16(3), 259. http://dx.doi.org/10.3390/mi16030259